

## Electronic Supplementary Information (ESI)

### Photocytotoxic Kinetically Stable Ruthenium(II)-N,N-donor Polypyridyl Complexes of Oxalate for Anticancer Activity Against HepG2 Liver Cancer Cells

Juhi Sayala<sup>a</sup>, Ekta Srivastava<sup>b</sup>, Priyaranjan Kumar<sup>a</sup>, Nitin Shukla<sup>a</sup>, Ashok Kumar<sup>b</sup>, Ashis K. Patra<sup>a\*</sup>

---

Authors address: <sup>a</sup>Department of Chemistry, Indian Institute of Technology Kanpur, Kanpur 208016, Uttar Pradesh, India, Email: [akpatra@iitk.ac.in](mailto:akpatra@iitk.ac.in)

<sup>b</sup>Department of Biological Science & Bioengineering Indian Institute of Technology Kanpur, Kanpur 208016, Uttar Pradesh, India

<sup>c</sup>Centre for Environmental Science and Engineering, Indian Institute of Technology Kanpur, Kanpur 208016, India

<sup>d</sup>Center for Nanosciences, Indian Institute of Technology Kanpur, Kanpur 208016, India

<sup>e</sup>The Mehta Family Centre for Engineering in Medicine, Indian Institute of Technology Kanpur, Kanpur 208016, India

<b><u>Contents</u></b>	<b>Page No.</b>
<b>Figure S1.</b> Solid-state FTIR overlay (in KBr pellets) for complexes <b>1–3</b> .	<b>3</b>
<b>Figure S2.</b> $^1\text{H}$ NMR of complex <b>1</b> .	<b>4</b>
<b>Figure S3.</b> $^1\text{H}$ NMR of complex <b>2</b> .	<b>5</b>
<b>Figure S4.</b> $^1\text{H}$ NMR of complex <b>3</b> .	<b>5</b>
<b>Figure S5.</b> Hydrolysis of complexes <b>2</b> and <b>3</b> in DMF-Tris buffer medium (pH 7.2).	<b>5</b>
<b>Figure S6.</b> Dark stability of complexes <b>2</b> and <b>3</b> in DMF using absorption spectroscopy.	<b>6</b>
<b>Figure S7.</b> Time-dependent $^1\text{H}$ -NMR spectra of the complex <b>1</b> .	<b>6</b>
<b>Figure S8.</b> Time-dependent $^1\text{H}$ -NMR spectra of the complex <b>2</b> .	<b>7</b>
<b>Figure S9.</b> Time-dependent $^1\text{H}$ -NMR spectra of the complex <b>3</b> .	<b>7</b>
<b>Figure S10.</b> Photoreactivity of the complex <b>3</b> in green light.	<b>8</b>
<b>Figure S11.</b> Green light irradiated time-dependent $^1\text{H}$ -NMR spectra of complex <b>1</b> .	<b>9</b>
<b>Figure S12.</b> Green light irradiated time-dependent $^1\text{H}$ -NMR spectra of complex <b>2</b> .	<b>10</b>
<b>Figure S13.</b> Green light irradiated time-dependent $^1\text{H}$ -NMR spectra of complex <b>3</b> .	<b>11</b>
<b>Figure S14.</b> Measurement of singlet oxygen generation by complex <b>1</b> using absorption spectroscopy.	<b>12</b>
<b>Figure S15.</b> Measurement of singlet oxygen generation by complex <b>2</b> using absorption spectroscopy.	<b>13</b>
<b>Figure S16.</b> Absorption spectral Singlet oxygen generation of the complex <b>3</b> .	<b>14</b>
<b>Figure S17.</b> Measurement of singlet oxygen generation of complexes <b>1, 2,</b> and <b>3</b> using emission spectroscopy.	<b>15</b>
<b>Figure S18.</b> DNA binding studies by ethidium bromide (EB) displacement assay for complexes <b>2</b> and <b>3</b> .	<b>16</b>
<b>Figure S19.</b> Fluorescence emission spectra of BSA upon addition of complex <b>2</b> .	<b>17</b>
<b>Figure S20.</b> Fluorescence emission spectra of BSA upon addition of complex <b>3</b> .	<b>18</b>

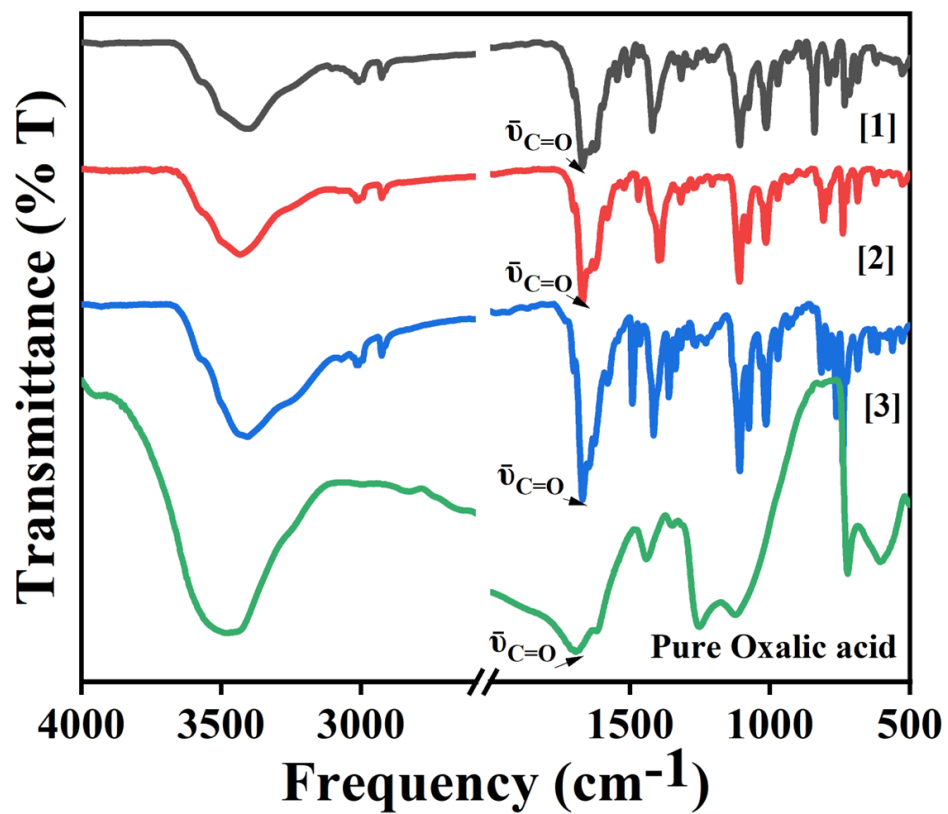


**Figure S1.** An overlay of the solid-state FT-IR spectra of the complexes **1**, **2**, **3** and oxalic acid in KBr pellet.

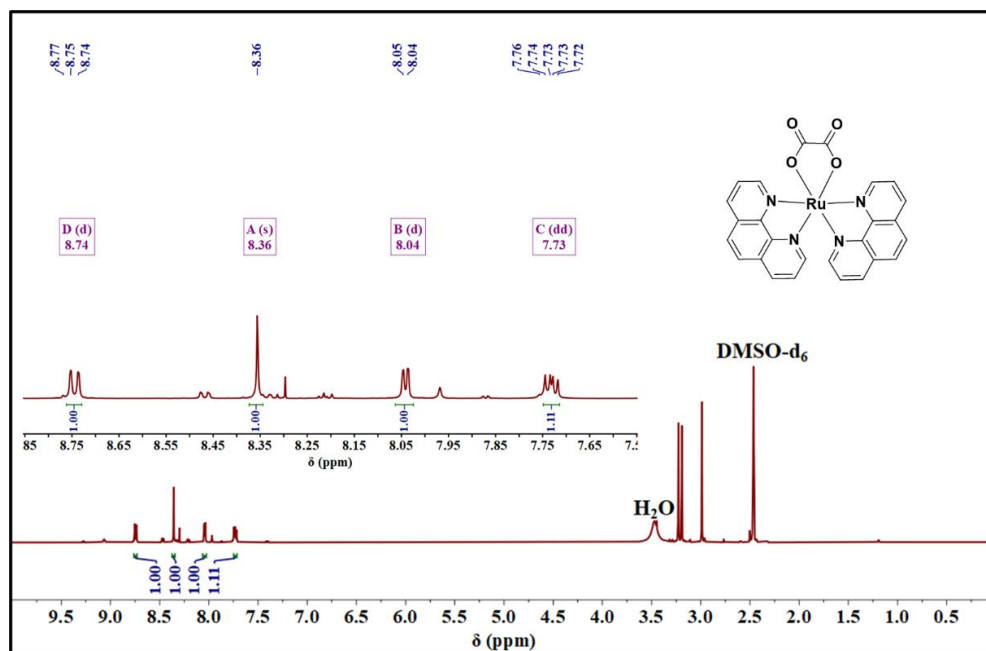


Figure S2.  $^1\text{H}$  NMR spectrum of complex  $[\text{Ru}^{\text{II}}(\text{phen})_2(\text{ox})]$  (**1**) (400 MHz,  $\text{DMSO-d}_6$ ).

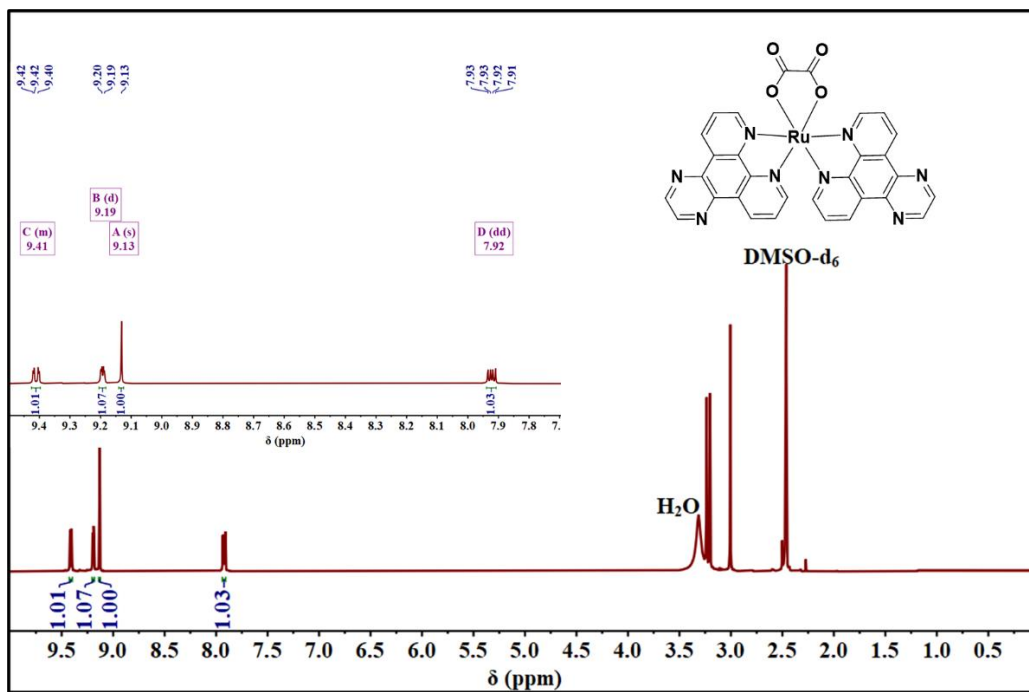
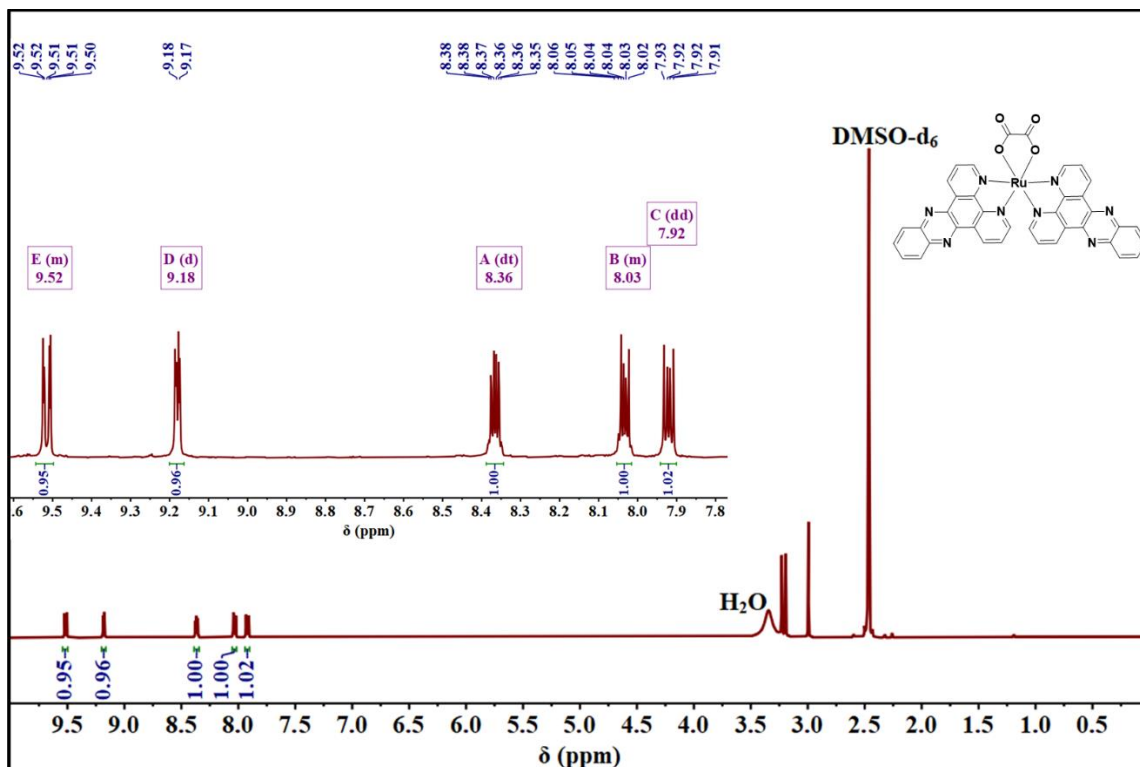
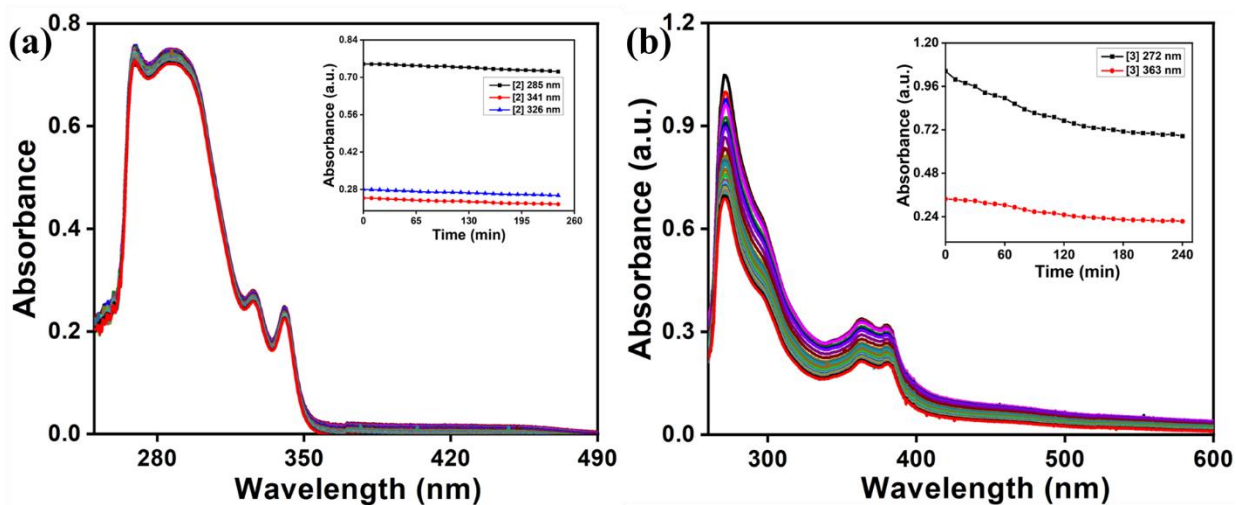


Figure S3.  $^1\text{H}$  NMR spectrum of complex  $[\text{Ru}^{\text{II}}(\text{dpq})_2(\text{ox})]$  (**2**) (400 MHz,  $\text{DMSO-d}_6$ ).



**Figure S4.**  $^1\text{H}$  NMR spectrum of complex  $[\text{Ru}^{\text{II}}(\text{dppz})_2(\text{ox})]$  (**3**) (400 MHz,  $\text{DMSO-d}_6$ ).



**Figure S5.** The electronic absorption changes of the complex **2** (a) and **3** (b) (48  $\mu\text{M}$ ) upon solvation for 240 min in the dark in 5% (v/v) DMF-5 mM Tris-HCl/NaCl buffer (pH = 7.2) mixture. Inset: Changes in  $A_{272\text{ nm}}$  and  $A_{363\text{ nm}}$  for complexes **2** and **3**.

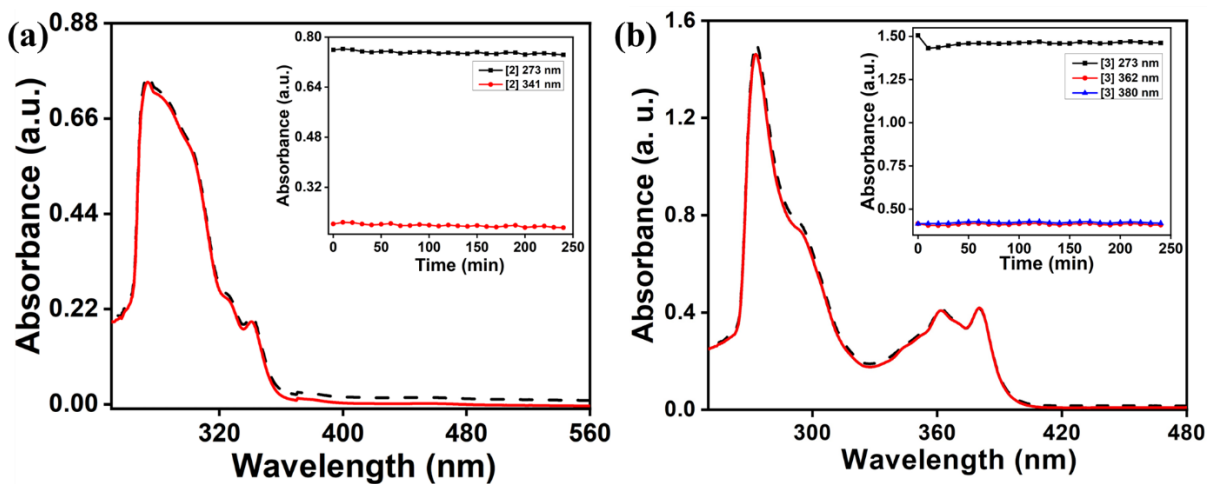


**Figure S6.** The electronic absorption changes of the complexes (48  $\mu$ M) **2** (a) and **3** (b) upon solvation for 0–240 min in the dark in DMF. Inset: Changes in  $A_\lambda$  for complexes **2** and **3**.

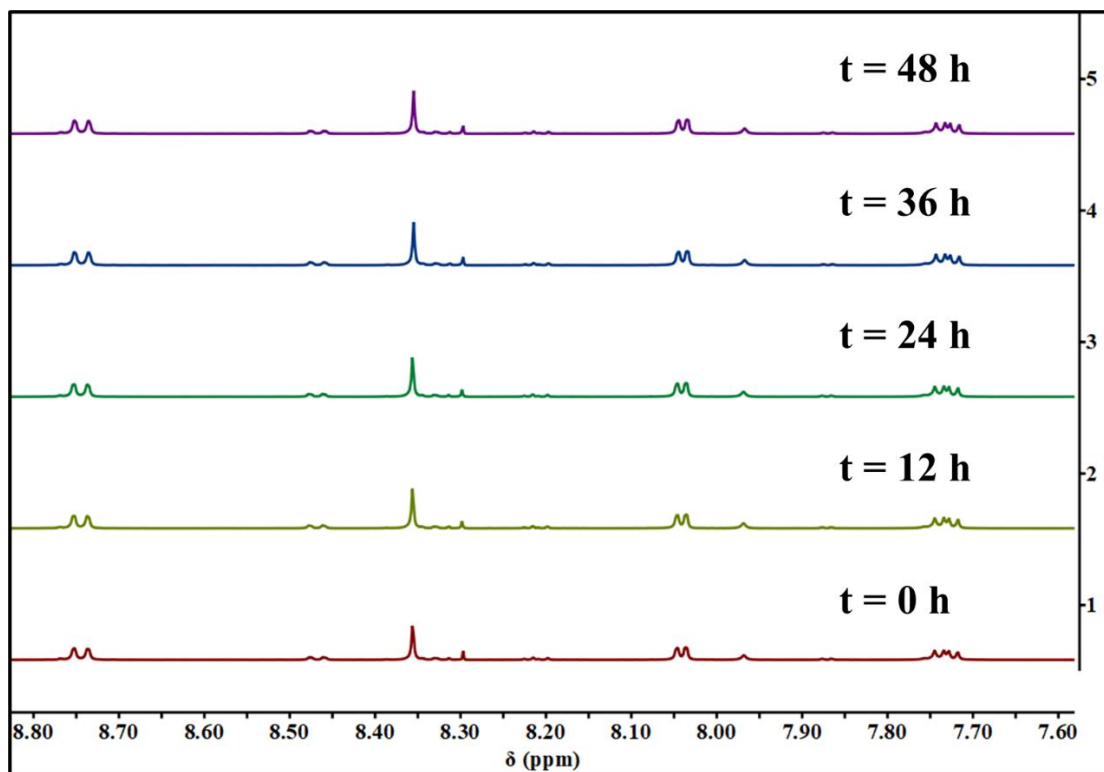


**Figure S7.** Time-dependent <sup>1</sup>H-NMR spectra of the complex **1** (DMSO-d<sub>6</sub>, 500 MHz). (a) Overlay of the region 7.50–8.50 ppm.

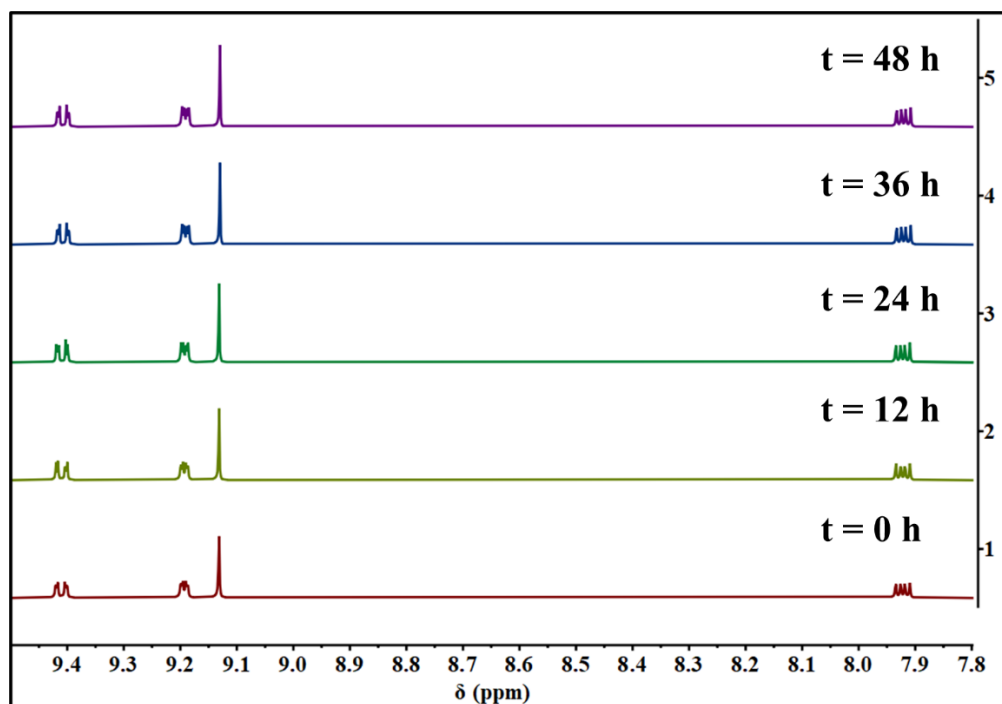


**Figure S8.** Time-dependent  $^1\text{H}$ -NMR spectra of the complex **2** (DMSO- $d_6$ , 500 MHz). (a) Overlay of the region 7.50-9.50 ppm.

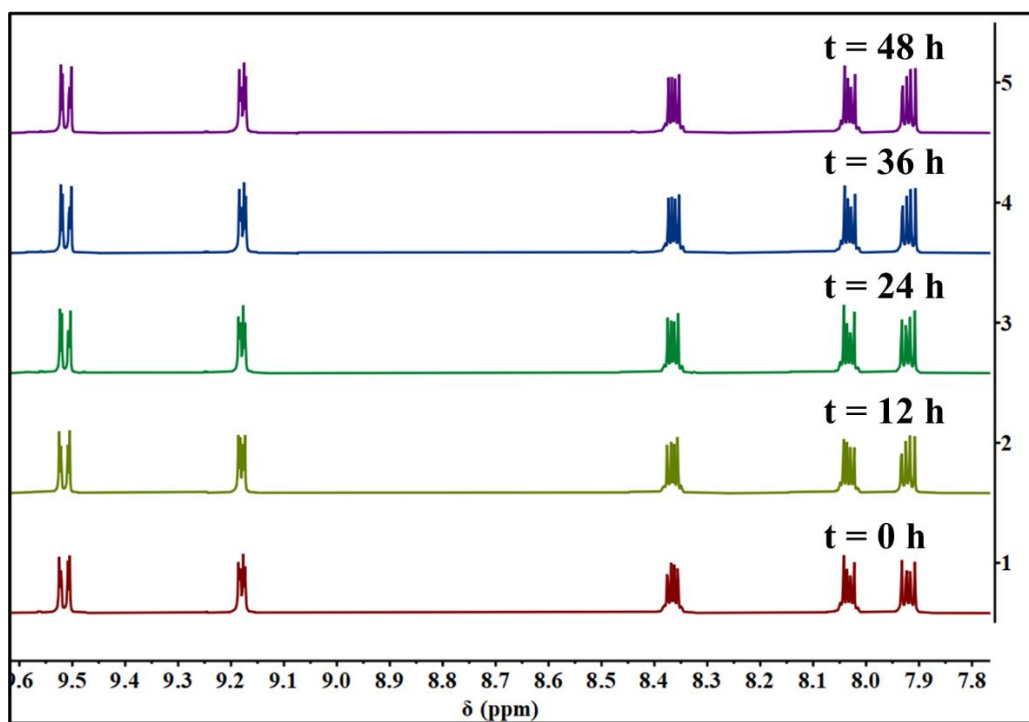


**Figure S9.** Time-dependent  $^1\text{H}$ -NMR spectra of the complex **3** (DMSO- $d_6$ , 500 MHz). (a) Overlay of the region 7.50-9.60 ppm.

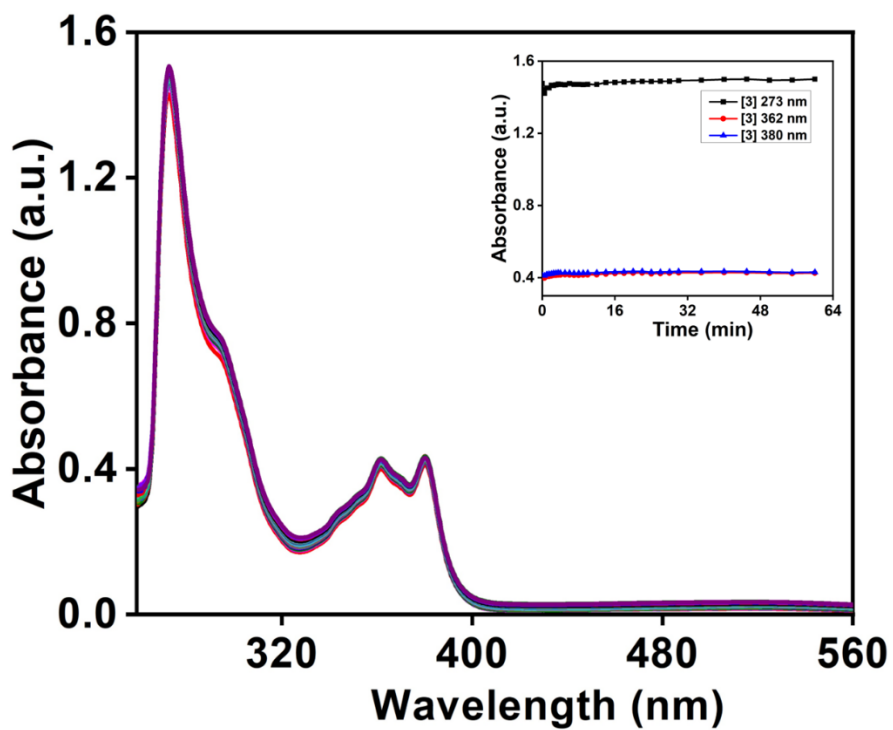


**Figure S10.** The green light ( $\lambda_{\text{irrad}} = 530 \text{ nm}$ ) LED (3 V, 158 lm@700 mA) induced spectral changes observed for the complexes **3** in DMF. Absorption spectral traces of complex **3** (24  $\mu\text{M}$ ) for the 0-60 min. Inset: Changes in  $A_{273 \text{ nm}}$ ,  $A_{362 \text{ nm}}$  and  $A_{380 \text{ nm}}$  of complex **3** with photoirradiation time.



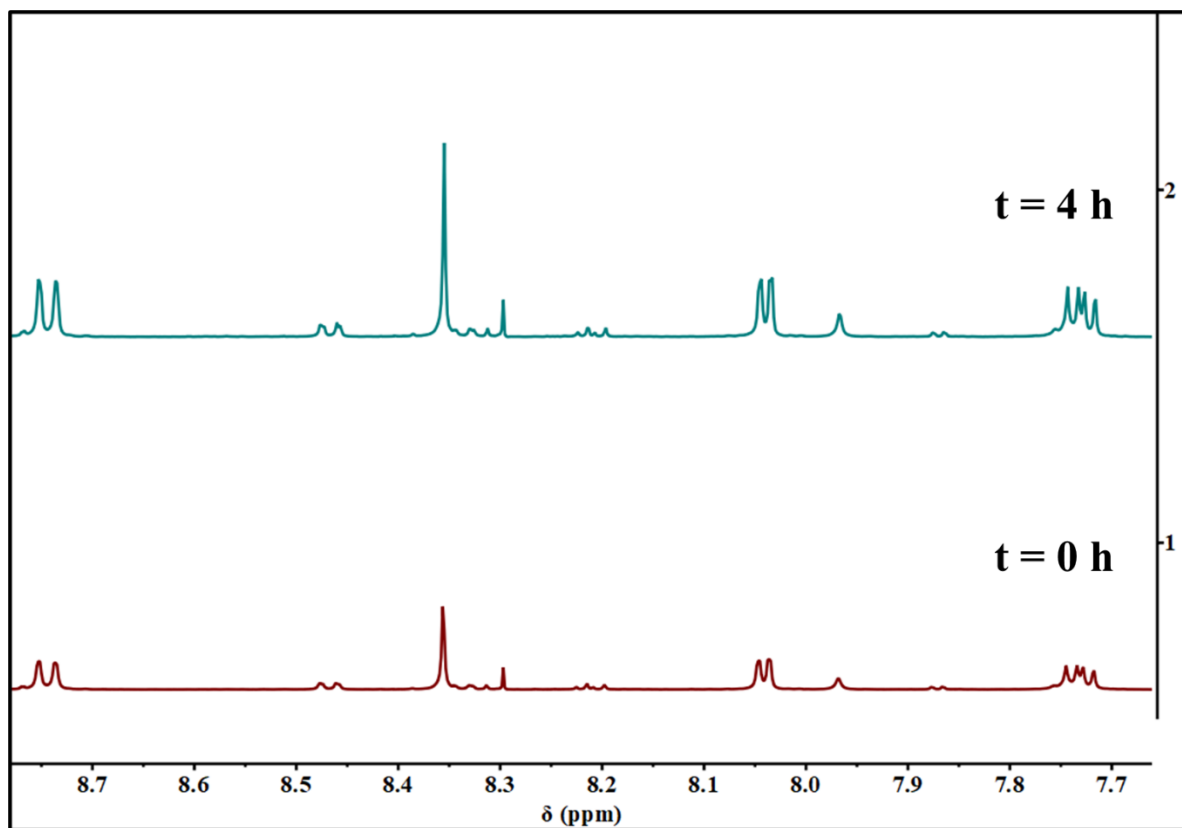


**Figure S11.** Green light ( $\lambda_{\text{irr}} = 530$  nm) irradiated Time-dependent <sup>1</sup>H-NMR spectra of the complex **1** (DMSO-d<sub>6</sub>, 500 MHz). (a) Overlay of the region 7.50-9.60 ppm. Maroon trace (0 h) and green trace (4 h).

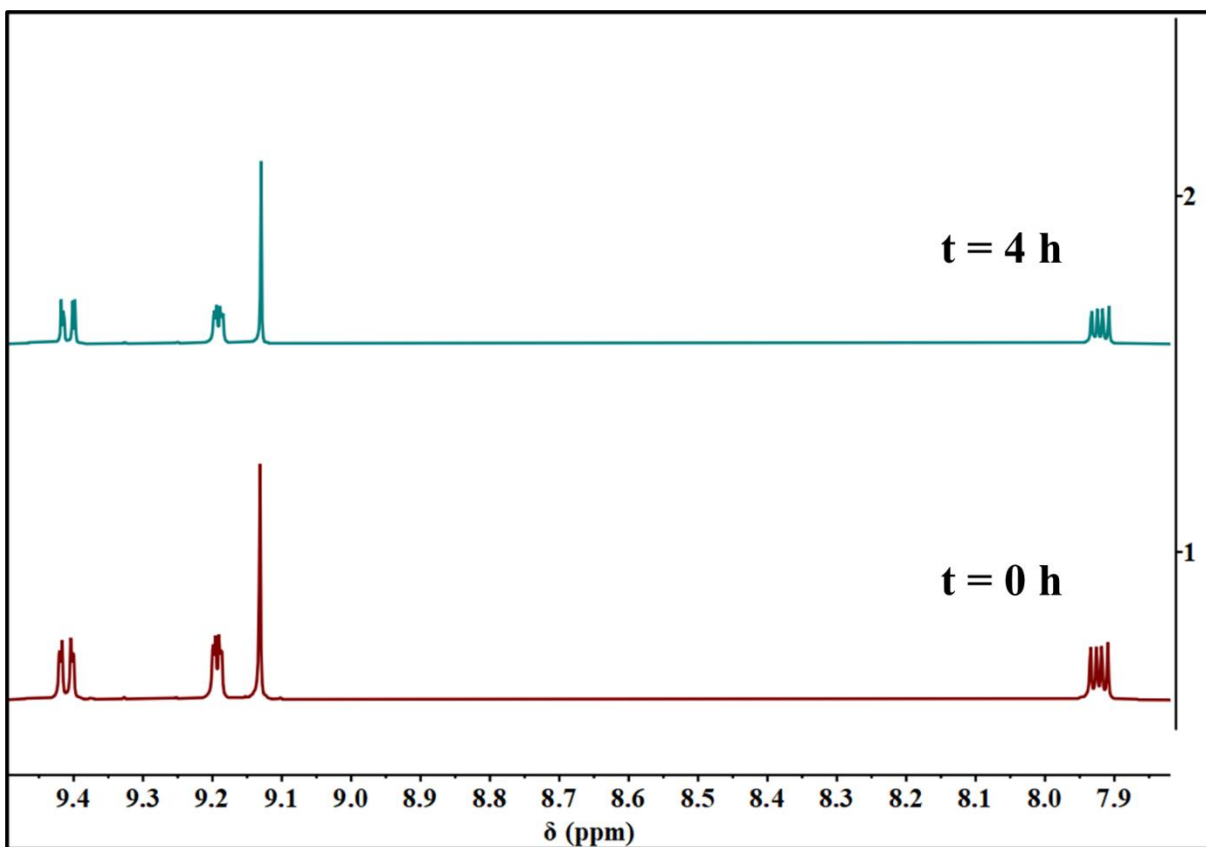


**Figure S12.** Green light ( $\lambda_{\text{irr}} = 530 \text{ nm}$ ) irradiated time-dependent <sup>1</sup>H-NMR spectra of the complex **2** (DMSO-d<sub>6</sub>, 500 MHz). (a) Overlay of the region 7.50-9.60 ppm. Maroon trace (0 h) and green trace (4 h).

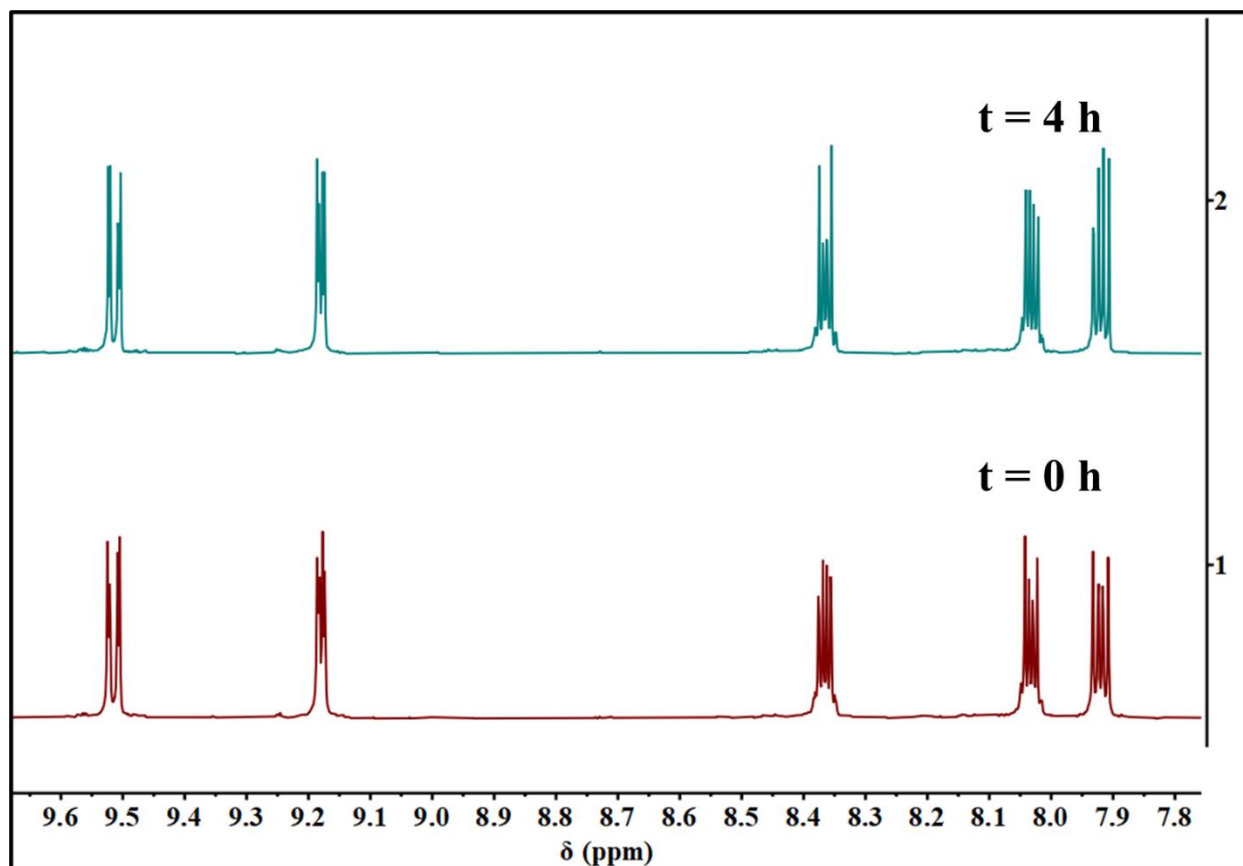


**Figure S13.** Greenlight ( $\lambda_{\text{irr}} = 530 \text{ nm}$ ) irradiated Time-dependent  $^1\text{H}$ -NMR spectra of the complex **3** (DMSO- $d_6$ , 500 MHz). (a) Overlay of the region 7.50-9.60 ppm. Maroon trace (0 h) and green trace (4 h).

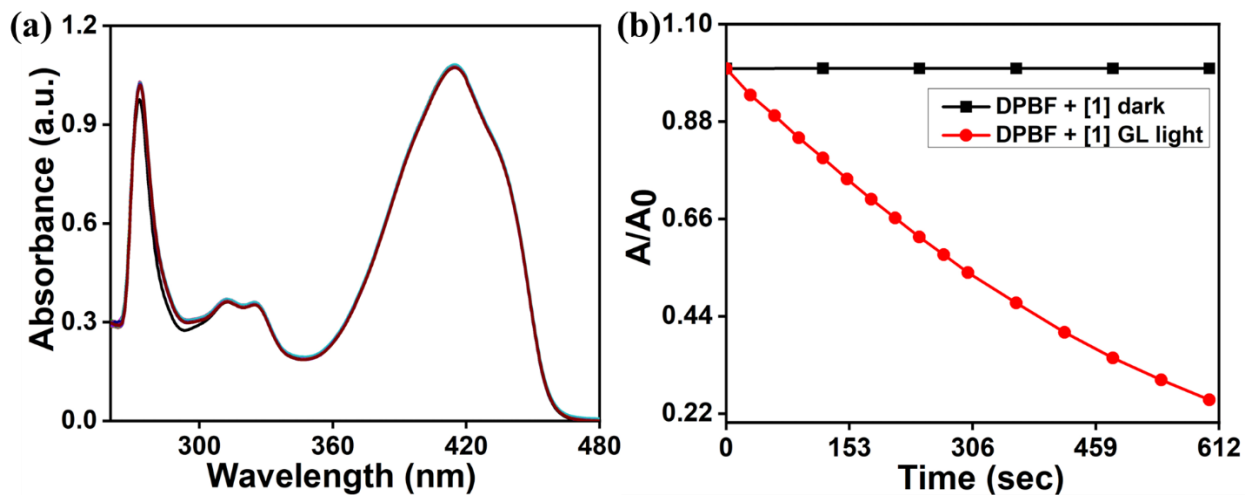


**Figure S14.** The absorption spectral profile of DPBF (50  $\mu\text{M}$ ) with **1** (10  $\mu\text{M}$ ) in the dark for 10 min shows the dark stability (a). Overlay of  $A/A_0$  at 414 nm for complex **1** with DPBF in the dark and green-light LED ( $\lambda_{\text{irr}} = 530 \text{ nm}$ , 3V, 158 lm@700mA) for 0–10 min (b). Spectra were recorded at 298 K in DMF solution.

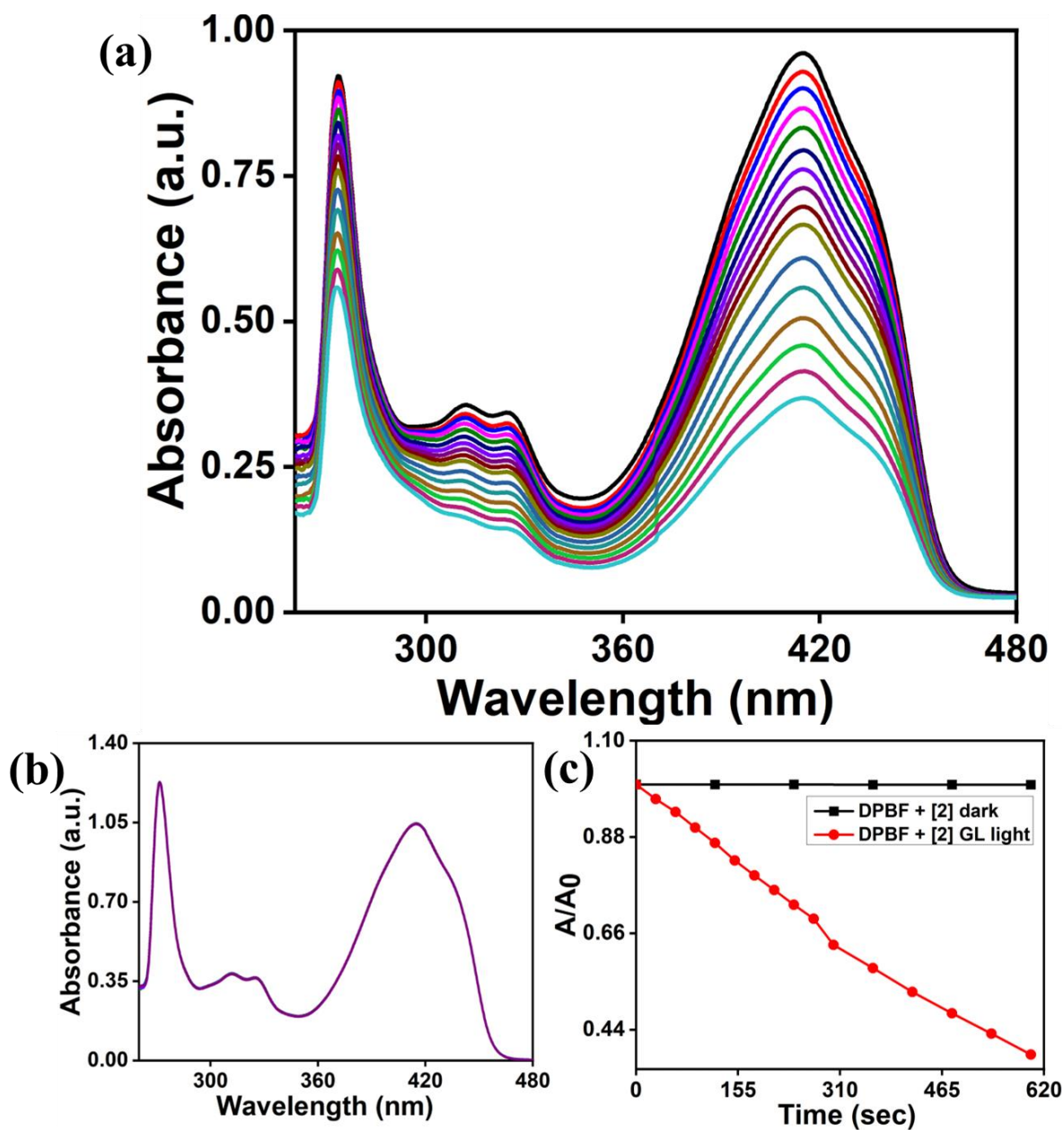


**Figure S15.** Absorption spectral profile of DPBF (50  $\mu\text{M}$ ) with **2** (10  $\mu\text{M}$ ) upon green light irradiation ( $\lambda_{\text{irr}}=530\text{ nm}$ ) for 10 min shows the  $^1\text{O}_2$  generation (a) and, in the dark for 10 min shows the dark stability (b). Overlay of  $A/A_0$  at 414 nm for complex **2** with DPBF in the dark and green-light LED ( $\lambda_{\text{irr}} = 530\text{ nm}$ , 3V 158 lm@700mA) for 0–10 min (c). Spectra were recorded at 298 K in DMF solution.

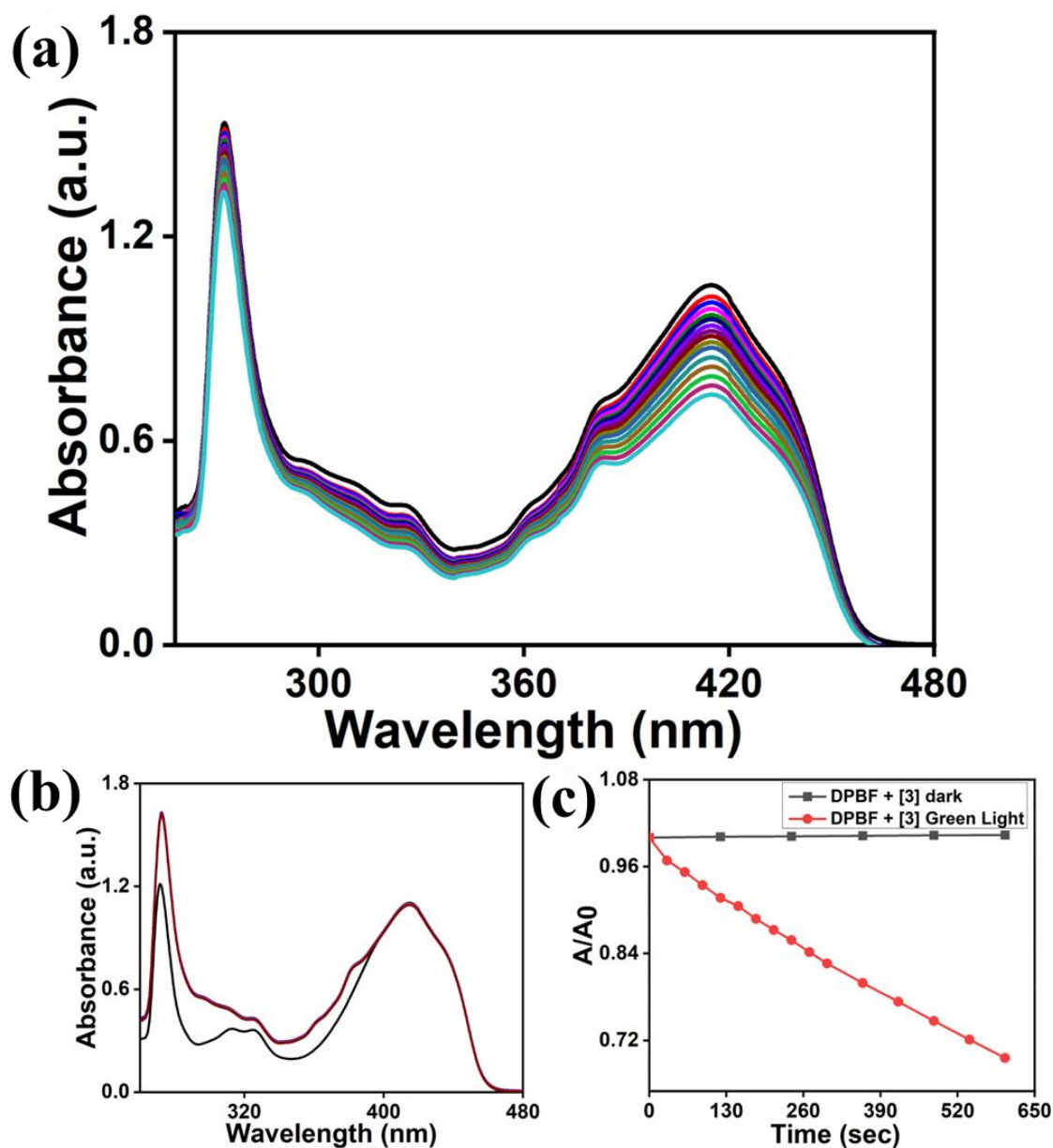


**Figure S16.** Absorption spectral profile of DPBF (50  $\mu\text{M}$ ) with **3** (10  $\mu\text{M}$ ) upon green light irradiation ( $\lambda_{\text{irr}} = 530 \text{ nm}$ ) for 10 min shows the  $^1\text{O}_2$  generation (a) and, in the dark for 10 min shows the dark stability (b). Overlay of  $A/A_0$  at 414 nm for complex **3** with DPBF in the dark and green-light LED ( $\lambda_{\text{irr}} = 530 \text{ nm}$ , 3V, 158 lm@700 mA) for 0–10 min (c). Spectra were recorded at 298 K in DMF solution.

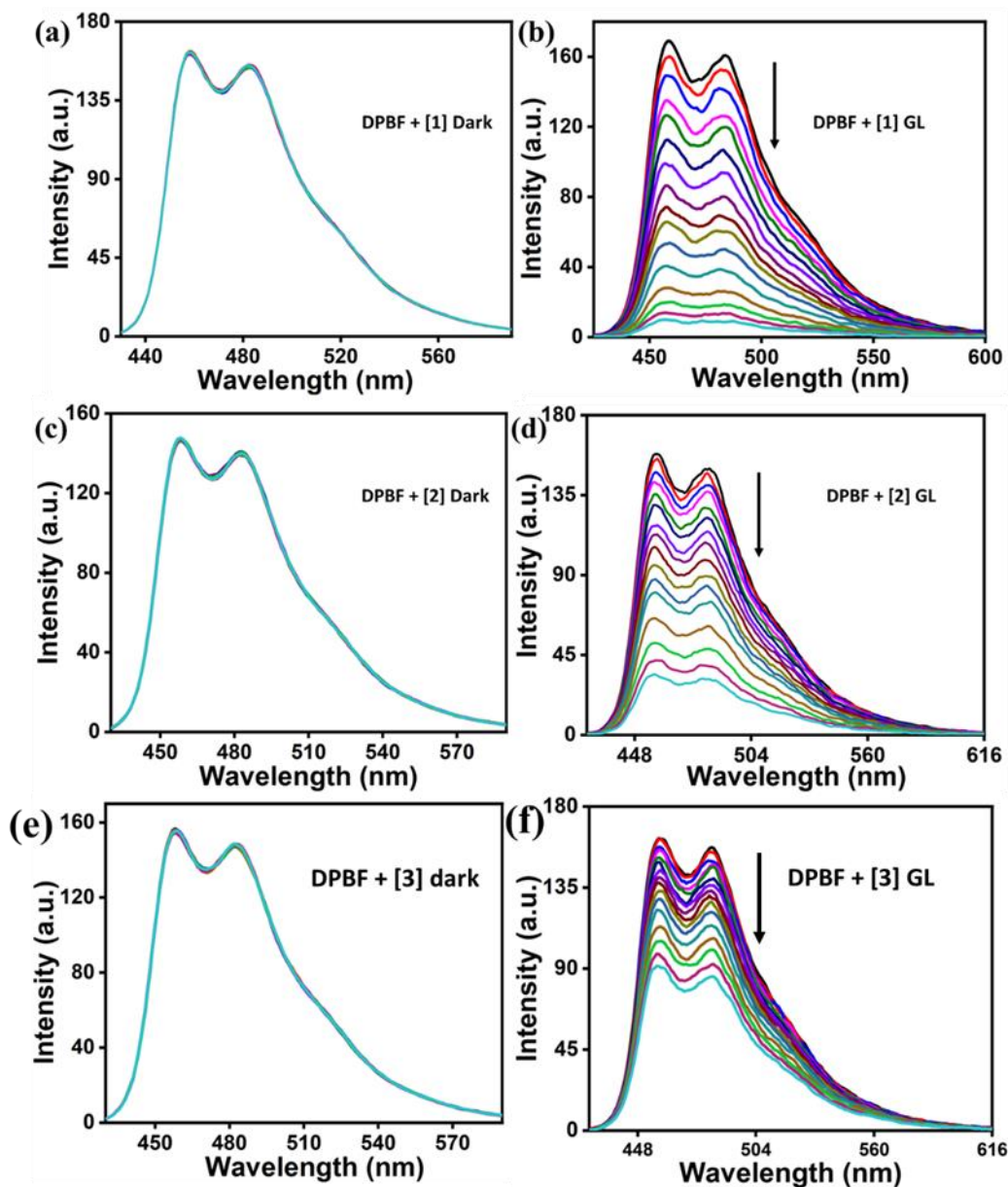


**Figure S17.** The emission spectral profile of DPBF (50  $\mu\text{M}$ ) with complexes **1**, **2** and **3** (5  $\mu\text{M}$ ) upon green light irradiation ( $\lambda_{\text{irr}} = 530 \text{ nm}$ ) for 10 min shows the  $^1\text{O}_2$  generation (b, d, f) and, in the dark for 10 min shows the dark stability (a, c, e), Green-light LED ( $\lambda_{\text{irr}} = 530 \text{ nm}$ , 3V, 158 lm@700 mA) for 0–10 min (c). Spectra were recorded at 298 K in DMF solution,  $\lambda_{\text{exc}}=415 \text{ nm}$ ,  $\lambda_{\text{em}}=460 \text{ nm}$ .

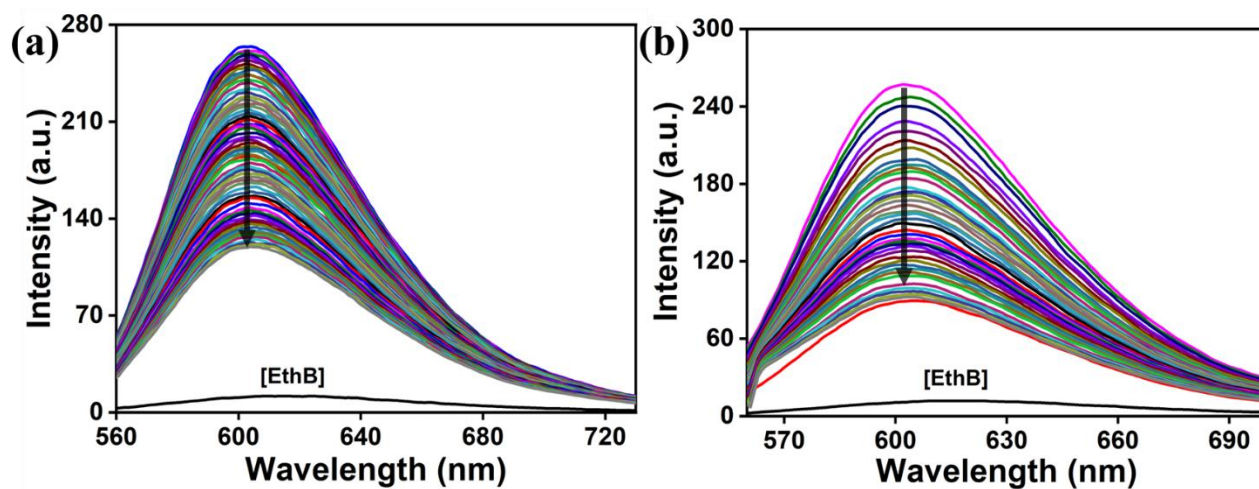


**Figure S18.** Emission spectrum of ethidium bromide (EB)-bound to DNA in the presence of complexes **2** (a) and **3** (b). ([EB] = 12.5  $\mu$ M, [DNA] = 15  $\mu$ M, [**2**] = 0-102  $\mu$ M, [**3**] = 0-45  $\mu$ M,  $\lambda_{\text{ex}}$  = 546 nm, Ex. and Em. slit width = 10 nm. The arrow shows the intensity change upon increasing complex concentration.



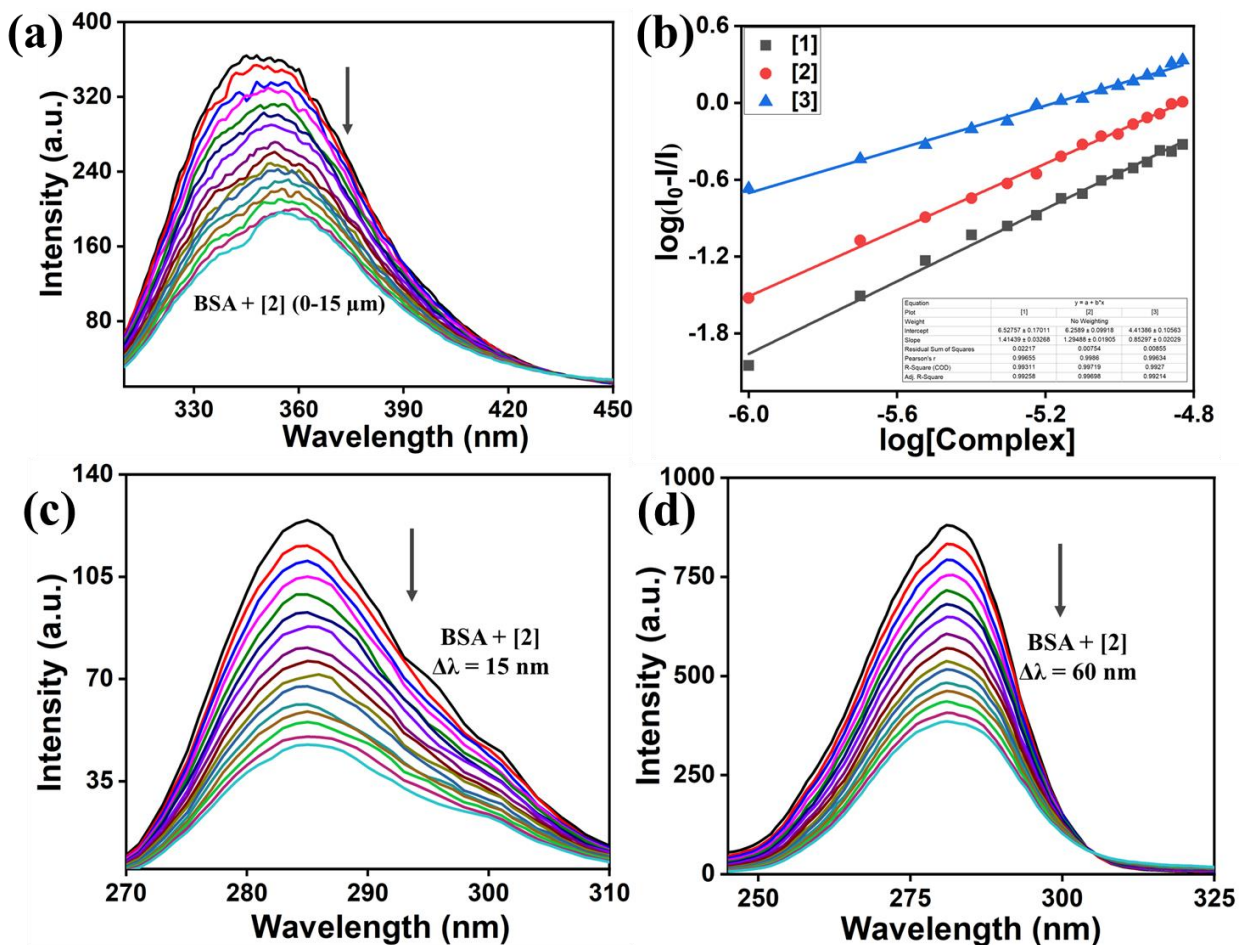


**Figure S19.** (a) The BSA (2 μM) binding of the complex 2 (0-15 μM) in 0.7% (v/v) DMF-5 mM Tris-HCl/NaCl buffer (pH = 7.2) at 298 K,  $\lambda_{\text{ex/em}} = 295/345$  nm and slit width = 10/5. (b) The Scatchard plot for the determination of the static equilibrium binding constant from the intercept and number of binding sites available ( $n$ ) from the slope of the plot. (c) The tyrosine fluorescence emission quenching of BSA upon increasing concentration of complex 2 using synchronous fluorescence studies. (d) The tryptophan fluorescence emission quenching of BSA upon increasing concentration of complex 2 using synchronous fluorescence studies.

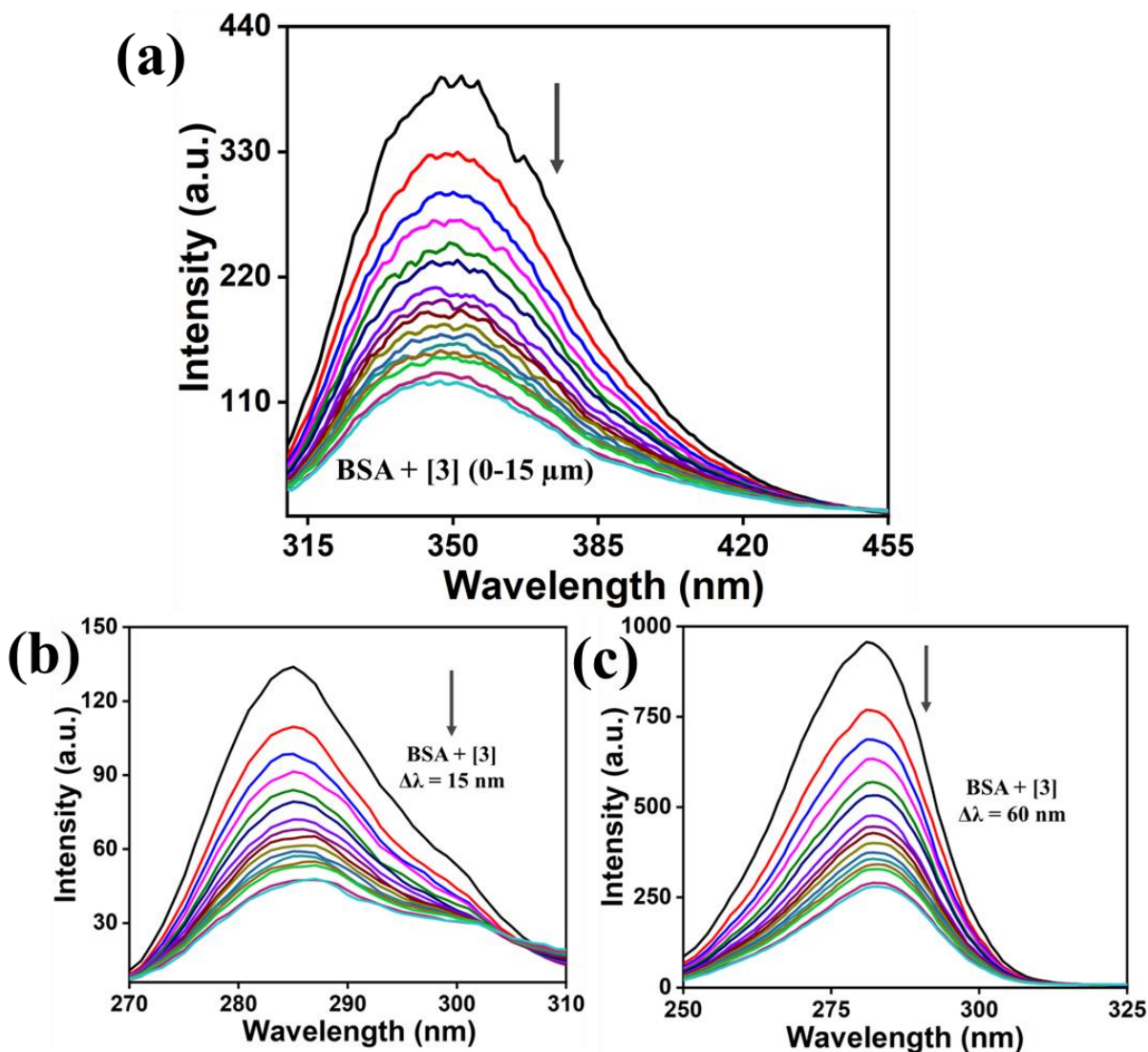


**Figure S20.** (a) The BSA (2 μM) binding of the complex **3** (0-15 μM) in 0.7% (v/v) DMF-5mM Tris-HCl/NaCl buffer (pH=7.2) at 298 K,  $\lambda_{ex/em} = 295/345$  nm and Ex./Em. slit widths= 10/5 nm. (b) The tyrosine fluorescence emission quenching of BSA upon increasing concentration of complex **3** using synchronous fluorescence studies. (d) The tryptophan fluorescence emission quenching of BSA upon increasing concentration of complex **3** using synchronous fluorescence studies.